AD-A045 419     UNIVERSITY OF. SOUTHERN CALIFORNIA LOS ANGELES  ELECTR--ETC  F/G 9/5
EVALUATION OF GALLIUM NITRIDE FOR ACTIVE MICROWAVE DEVICES.(U)
AUG 77   M GERSHENZON                                 N00014-75-C-0295

UNCLASSIFIED                                                        NL

| OF |
AD
A045419

END
DATE
FILMED

11 -77

DDC

PROGRESS REPORT


ONR Contract N-00014-75-C-0295



EVALUATION OF GALLIUM NITRIDE
FOR ACTIVE MICROWAVE DEVICES

M. Gershenzon
Electronic Sciences Laboratory
University of Southern California
University Park
Los Angeles, California    90007

August 1977


Contract Authority NR 243-004

D D C

OCT 20 1977

B

| REPORT DOCUMENTATION PAGE | | READ INSTRUCTIONS<br>BEFORE COMPLETING FORM |
|---|---|---|
| 1. REPORT NUMBER | 2. GOVT ACCESSION NO. | 3. RECIPIENT'S CATALOG NUMBER |
| 4. TITLE (and Subtitle)<br>"Evaluation of Gallium Nitride for Active Microwave Devices" | | 5. TYPE OF REPORT & PERIOD COVERED<br>Annual Technical repts<br>Mar 76 - Aug 77 |
| | | 6. PERFORMING ORG. REPORT NUMBER |
| 7. AUTHOR(s)<br>M. Gershenzon | | 8. CONTRACT OR GRANT NUMBER(s)<br>N00014-75-C-0295 |
| 9. PERFORMING ORGANIZATION NAME AND ADDRESS<br>Electronic Sciences Laboratory<br>University of Southern California<br>Los Angeles, CA 90007 | RR 021-02 | 10. PROGRAM ELEMENT, PROJECT, TASK AREA & WORK UNIT NUMBERS<br>PE 61153N<br>RR 021-02-03<br>NR 243-004 |
| 11. CONTROLLING OFFICE NAME AND ADDRESS<br>ONR Code 427 Arlington, VA 22217 | | 12. REPORT DATE<br>August, 1977 |
| | | 13. NUMBER OF PAGES<br>32 |
| 14. MONITORING AGENCY NAME & ADDRESS(if different from Controlling Office) | | 15. SECURITY CLASS. (of this report)<br>UNCLAS |
| | | 15a. DECLASSIFICATION/DOWNGRADING SCHEDULE |

16. DISTRIBUTION STATEMENT (of this Report)

Approved for public release; distribution unlimited

17. DISTRIBUTION STATEMENT (of the abstract entered in Block 20, if different from Report)

18. SUPPLEMENTARY NOTES

ONR Scientific Officer
Tel. (202) 692-4218

361 620

19. KEY WORDS (Continue on reverse side if necessary and identify by block number)

Gallium Nitride, Vapor phase epitaxy, crystal growth

20. ABSTRACT (Continue on reverse side if necessary and identify by block number)

In an attempt to minimize the high native donor density and the structural defects which lead to high field breakdown, so that high field drift velocity measurements can be made, a high pressure (10,000 atm), high temperature (1500°C) system is being set up to grow, anneal

DD FORM 1473 EDITION OF 1 NOV 65 IS OBSOLETE
1 JAN 73
S/N 0102-014-6601 |

and diffuse GaN under equilibrium $N_2$ pressures, rather than by the non-equilibrium $NH_3$ vapor phase method currently used to prepare GaN. The system should be completely operational within 4 months. A second chemical vapor deposition apparatus designed to grow 50μ *micrometers* crystals on R-plane sapphire at 1050 °C is now working and uniform crystals are being grown routinely. Due to non-planar nucleation and growth, these crystals exhibit decorated low angle grain boundaries, some of which crack by differential thermal contraction during cool-down, and stacking faults and random small-scale precipitation in regions paralleling the linear surface topology. Light scattering from these regions colors the bulk samples. Slow growth rates eliminate the precipitated regions and tend to reduce the number of low angle boundaries and associated cracks. However, planar growth, which proceeds very s        on $(10\bar{1}0)$ sapphire or on self-nucleated whiskers eliminated virtu         l these defects. These vapor grown crystals have been characterized by low temperature bound exciton spectra, revealing the presence of at least two shallow donors (30-40 meV), two "shallow" acceptors (200-300 meV) and one much deeper acceptor. Attempts are under way to identify the chemical nature of these centers.

ACCESSION for

| NTIS | White Section |
| DDC | Buff Section | □ |
| UNANNOUNCED | | □ |
| JUSTIFICATION | | |

BY
DISTRIBUTION/AVAILABILITY CODES
Dist.          or SPECIAL

A

# TABLE OF CONTENTS

## INTRODUCTION

Gallium nitride is predicted to be a good candidate for active microwave devices based on transit-time limited drift of electrons and holes produced by pair production at high fields. The high direct bandgap, the low electron effective mass and the small mass of nitrogen in GaN predict a figure of merit for GaN as a microwave power amplifier (breakdown voltage squared times electron saturated drift velocity) that is at least a factor of 20 greater than that for Si.

Most of the previous work on GaN has been ultimately aimed at producing electroluminescent devices for the visible and near ultra-violet, but our goals have been to prepare appropriate materials from which structures can be made to measure the high field saturated drift velocity and the pair production threshold, as well as to delineate the physics, chemistry, metallurgy and device technology that would be needed to use GaN as a semiconductor.

There are three basic problems, probably not unrelated, which set GaN apart as an unusually difficult semiconductor to work with. First, the true 3-phase maximum melting point is about 2,000°C under an equilibrim $N_2$ pressure of perhaps 40,000 atm. Second, no low resistivity p-type material has ever been conclusively demonstrated. Third, the purest material is degenerate n-type at room temperature, with a carrier concentration of 1-5 x $10^{18}$ $cm^{-3}$. This donor level may, however, be compensated with acceptors to yield high resistivity material, but of low electron mobility. Semiconductors can normally be grown at temperatures as low as 30% below the melting point either from solution (liquid phase epitaxy) or from a gas phase (chemical vapor deposition). Below this limit, thermal motion is too slow to allow single crystal growth at

acceptable rates. At this limit for GaN, 1200°C, the equilibrium $N_2$ pressure, 3,000 atm. is already much too great to allow crystal growth in any normal type of apparatus. These high numbers are basically due to the great stability of the $N_2$ molecule. To avoid this problem GaN can be prepared from an "activated" source of nitrogen, either from a low pressure electric discharge in $N_2$ or by the use of $NH_3$. The activated species in the discharge are either N atoms or, more likely, excited states of $N_2$ molecules. To avoid de-excitation of these species before their impingement on a growing GaN surface, the mean free paths must be long. This requires low pressures and hence leads to very slow growth rates. The use of $NH_3$ as the active species is based on two facts. First, at about 1000°C, because of the high strength of the N-N bond, $N_2$ is much more stable than $NH_3$; starting from pure $NH_3$ only ~10 <u>torr</u> of $NH_3$ should co-exist in equilibrium with about 1,000 <u>atm</u> of $N_2$ and $H_2$. However, the kinetics for the homogeneous dissociation of $NH_3$ into $N_2$ and $H_2$ are very slow below 1100°. Hence small pressures of $NH_3$ can be used up to about 1100° in place of the corresponding large pressures of $N_2$ required, about 600 atm at 1100°. Slow CVD growth is then possible by reacting $NH_3$ with a vapor containing Ga, either as a halide or an organo-metal species. This leads to a non-equilibrium growth rate. For GaX as the Ga containing molecule, the forward reaction is GaX + $NH_3$ → GaN + ..., whereas the back reaction is not the reverse of this, but rather the decomposition to $N_2$, GaN → Ga + $N_2$. Hence growth or decomposition is determined by a kinetic balance between these two reactions, and a zero-growth rate does not correspond to any single equilibrium reaction. We suspect that the third basic problem noted above is a direct consequence of this conclusion. As discussed below, we are led to believe that the very high donor density characteristic of crystals grown from $NH_3$ is due to a native defect,

probably a N vacancy, rather than to any chemical impurities. For true equilibration with a $N_2$ ambient, its concentration would depend on the $N_2$ pressure as well as the temperature. However, for growth via $NH_3$, the $N_2$ pressure is virtually zero, predicting a maximal concentration of N vacancies from that equilibrium. Since the $NH_3$ reaction is not an equilibrium one, it is difficult to predict how high a vacancy density should be expected from that reaction.

Although compensation can decrease the free electron concentration, it does so at the expense of mobility. If we are to make definitive saturated drift velocity and pair production measurements we must lower the carrier density about a factor of 10 below current $NH_3$ grown material while maintaining the high mobility (100-150 $cm^2 v^{-1} sec^{-1}$). Furthermore, if GaN is ever to become a "normal" semiconductor material, we would have to learn to prepare even purer material.

The primary goal of our last two proposals therefore, has been the growth and equilibration of GaN under equilibrium $N_2$ pressures at temperatures up to about 80% of the expected true melting point, to measure the intrinsic defect density as a function of temperature and $N_2$ pressure, as well as to alleviate various other growth defects to be discussed below.

This report will also show that the second basic problem mentioned, the present unattainability of low resistivity p-type material is due to the fact that the ionization energies for the simple expected acceptors in GaN appear to be too deep (0.20 eV) to exhibit significant ionization at room temperature.

This annual report will first briefly summarize our work over the previous two years, then discuss this year's progress on the high-temperature, high pressure system, a defect analysis of our $NH_3$-GaCl CVD crystals grown on R-plane sapphire and donor and acceptor characterization from

-4-

low temperature luminescence.

## SUMMARY OF PAST PROGRESS

Good single crystal growth of GaN at 1050°C by the vapor phase reaction of $NH_3$ and GaCl (from HCl and liquid Ga) was demonstrated on sapphire substrates by optimizing temperature, flow rates, growth chamber geometry and substrate orientation and surface preparation. R-plane ($10\bar{1}2$) sapphire yielded the most consistent results with basal plane (0001) sapphire not much worse. Using chemically etched sapphire (hot $H_3 PO_4$) a two-stage growth was necessary: a slow < 30μ/hr nucleating growth step followed by a more rapid 100μ/hr growth rate. We showed that the first slow growth step could be eliminated by pre-annealing the sapphire in $H_2$ at 1200-1300° just before growth. Thin as-grown layers (10μ) exhibited n-type carrier densities as high as $10^{20} cm^{-3}$ whereas thicker layers (50μ) had lower densities, $5 \times 10^{19} cm^{-3}$. Hence we decided to attempt to grow fairly thick samples for this reason as well as to simplify sample removal from the substrate. By re-optimizing flow rates and growth chamber geometry, we learned to grow 1 x 2 cm samples uniformly 2-3mm thick routinely (and some thicker than 10mm). However, the carrier density remained at $5 \times 10^{19} cm^{-3}$. Chemical analyses, doping experiments and optical absorption showed only three impurities present in this concentration, Si, O and H. Of these, only Si was shown to be a shallow donor. Hence the Si was removed by using higher grade starting gases and particularly, by using an alumina liner in the growth system to prevent any reaction between the HCl and the fused silica envelope. As a result, the measured Si concentration fell to less than $2 \times 10^{18} cm^{-3}$ but the electron density dropped only to $3-5 \times 10^{18} cm^{-3}$. Further purification had no effect. CVD growth from trimethyl-Ga and $NH_3$ yielded similarly

doped crystals. Hence we concluded that the dominant shallow donor was now a native defect, possibly a N vacancy.

We set up a system to measure the high field saturated drift velocity by the Ryder pulsed method and showed that our best samples were not good enough for measurements at the high fields necessary. First, to avoid thermal effects, we require samples with carrier densities of $\sim 10^{17} cm^{-3}$, more than a factor of 10 lower than our as-grown crystals without lowering the mobility already available ($> 100 cm^2 v^{-1} sec^{-1}$). Second, the samples exhibited both bulk and surface breakdown at fields only slightly greater than $10^3 V/cm$. We tried compensation with acceptors, e.g. Li, which can be diffused under $NH_3$ at temperatures below the dissociation limit of $NH$. This does drop the carrier density the required amount, but the mobility dropped precipitously. Furthermore, such diffusions heavily decorate dislocations and especially low angle grain boudnaries aggrevating the breakdown problem. Microscopic observation of the breakdown process in as-grown crystals then showed that the breakdown was clearly associated with microcracks and with precipitates, both as random particles and decorating low angle grain boudanries.

Previous reports summarize our other measurements, including resistivity, Hall effect, ohmic contacts, polishing, etching, optical absorption, etc. and will not be treated here.

Our progress this year has been aimed along three lines; high-pressure, high-temperature equilibration and growth under $N_2$ to minimize the intrinsic donor, a detailed defect structure analysis of current CVD grown crystals to avoid breakdown at high fields, and a new low temperature luminescence technique to define and characterize the shallow levels present in such material, both intrinsic and extrinsic.

## HIGH PRESSURE-HIGH TEMPERATURE SYSTEM

The system designed to process and grow GaN under an ambient of $N_2$ gas capable of 1500°C and 10,000 atm consists of the following major sub-systems:

A manually operated single stage piston-cylinder compressor rated for 4,000 atm.

A semi-automatic 3-stage intensifier with a capability of up to 14,000 atm.

A small TZM (titanium-zirconium-molybdenum alloy) autoclave with an external furnace for operation to 1100° and 3,000 atm.

A large internally heated, two-zone high pressure vessel (for annealing, liquid phase crystal growth and diffusion) rated at 1500° and 10,000 atm.

A similar vessel, with identical ratings, but with the addition of appropriate electrical feed-throughs for differential thermal analysis and in situ resistivity measurements.

Because (1) funding under the present one year contract was two months late in arriving, (2) the long lead time necessary for filling these orders, and (3) the fact that the 3-stage intensifier arrived with extensive damage during shipment, the complete system is not yet operational. The small single-stage compressor and the TZM vessel are set up. The large 3-stage intensifier is now being repaired and the first internally-heated vessel is now being connected to the system. The second large vessel has not yet been received; we expect shipment in October. Hence, we are just starting preliminary annealing experiments in the TZM vessel, and hope to be using the complete system by January 1, 1978.

## CRYSTAL GROWTH AND ANNEALING

A second CVD growth apparatus is now operational. This has been designed to grow routinely standard GaN crystals, 50μ thick on R-plane sapphire from $NH_3$ and GaCl. This system has better flow and temperature control than the original apparatus, each of the incoming gasses flows through a calcia-stabilized zirconia oxygen pump to remove (or introduce known quantities of) oxygen. Si contamination is minimized by a long high purity alumina liner and the apparatus is designed for easy sample insertion and removal. The standard crystals now being grown consistently 1 x 2 cm x 50μ exhibit a carrier concentration of 2-5 x $10^{18} cm^{-3}$ and a mobility averaging over 100 $cm^2 v^{-1} sec^{-1}$. The defect structure of such crystals is described in detail in the next section.

The first CVD apparatus has now been freed for a series of experiments designed to improve the perfection of CVD crystals by investigating growth on other substrate orientations, by trying other substrate materials in conjunction with an attempt to grow at lower temperatures and to dope the crystals with expected shallow donors and acceptors as an adjunct to our ion implantation studies, using low temperature bound exciton luminescence to characterize these centers, as described later.

We have repeated a series of annealing experiments in 1 atm of flowing $NH_3$ between 1000 and 1200° in order to establish a reproducible base line for the ion implantation experiments and the high pressure anneals in $N_2$. As expected, above 1100° the dissociation of $NH_3$ is very rapid and the samples begin decomposing. Between 1000 and 1100° annealing does not alter the carrier density. At 1100°, however, the luminescence efficiency of the low temperature bound exciton spectrum increases significantly. At the same time some surface crystal regrowth

-8-

is apparent. Thus, the crystals originally grown at 1050° can be somewhat improved by an 1100° anneal, at least to the extent of decreasing the effect of non-radiative recombination centers.

## DEFECT STRUCTURE AND CRYSTAL PERFECTION OF STANDARD GaN CRYSTALS

We have recognized previously that CVD ($GaCl-NH_3$) grown GaN on sapphire contains micro-cracks, low angle grain boundaries, precipitates, voids and stacking faults. These limited the high field breakdown of the crystals, they seemed to affect the optical transmission, and we were concerned that the effective carrier densities and mobilities might be influenced by such defects. Accordingly, we undertook a detailed structural analysis program to characterize our standard CVD crystals grown on R-plane sapphire at 1050° and to compare these results with those obtained by varying growth rates and substrate orientation. In addition we compared these results with those obtained from whiskers, small crystallites which grew off the $NH_3$ inlet tube in the reaction zone.

We started with 200μ thick crystals grown very slowly (1-2μ/hr) on R-plane sapphire ($\bar{1}012$). Laue x-ray patterns indicate that the GaN grows as a ($11\bar{2}0$) plane on this surface, its c-axis in the growth plane. This change in orientation is consistent with the best lattice match between Ga and N sites with Al and O sites at the interface. X-ray diffraction indicates that all the GaN is oriented very close to this direction; there are no high angle grain boundaries. The surface topography of the GaN is not planar; ridges and valleys are oriented approximately perpindicular to the c-axis. Using optical microscopy, transmitted light reveals the presence of linear decorated faults running parallel to the c-axis. Figures 1 and 2 show the transmission patterns through an

|←5000 μ →|     FIG. 1



|←300 μ →|     FIG. 2
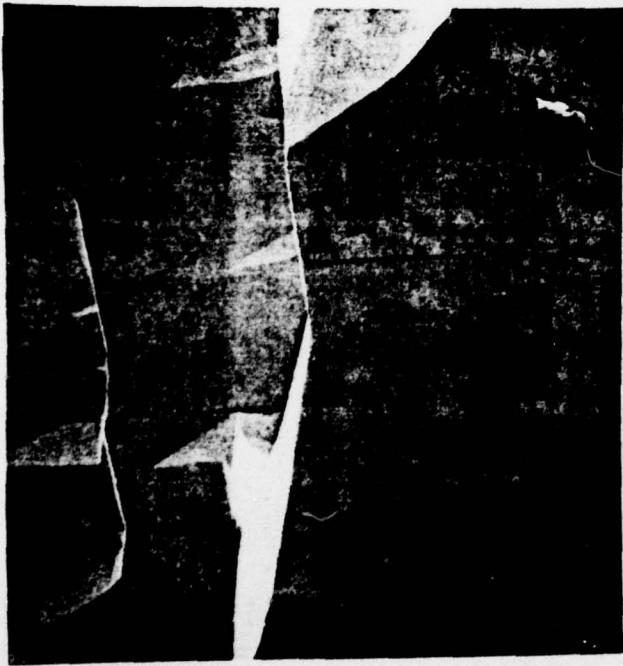


|←500 μ →|     FIG. 3  ——→ [0001]



|←10 μ →|     FIG. 4

unpolished crystal, so that it is obvious that these linear faults traverse
more than one ridge.  Scanning electron microscopy of such samples (Fig. 3)
reveals a series of cracks (open about 1/2μ) also parallel to the c-axis.
Re-examining such samples under high resolution in the optical micro-
scope, comparing transmitted light patterns with surface reflection
patterns, indicates that all the cracks are correlated with the bulk
fault lines, but that not all the fault lines have cracked.  In addition,
from observations on unpolished samples, these cracks are not stopped
by the surface growth ridges.  Several unpolished, unetched samples
were cleaved along these cracks and the cleaved surfaces examined by
the scanning electron microscope in the secondary emission mode.  Figure 4
shows such a typical cleavage plane, containing a series of bubble-like
particles.  These are spread out, as a liquid, wetting the GaN surface.
Hence they must be metallic Ga, molten by the heat of the electron beam.
By focussing the beam on one of these particles and using the instrument
in the x-ray energy dispersive mode, these particles were indeed shown to
be free Ga.  If the crystals are cleaved perpendicular to the c-axis no
precipitates are observed.  Hence the cracks occur on some Ga-decorated low
angle grain boundary planes running parallel to the c-axis.  Since the
cracks cross many ridges and valleys of the surface topology, they probably
do not occur at the growth temperature.  Rather, they must be due to
the difference in thermal contraction between GaN and sapphire as the
crystals are cooled to room temperature.  GaN has a higher thermal
expansion coefficient than sapphire.  Hence on cooling down the GaN should
be in compression, the sapphire in tension.  In agreement with this con-
clusion, for very thick (>2mm) GaN layers, the sapphire substrate is
always very cracked and for thinner GaN layers the cracks in the GaN

originate at the surface (maximum compression), but rarely propagate through to the sapphire interface. These cracks and associated decorated low angle grain boundaries are always observed on 50μ to 2mm thick GaN grown on R-plane sapphire. Other sapphire orientations (parallel to $\overline{1}012$, see below) produce crystals with fewer cracks, and very slow growth rates. < 1μ/hr, reduce the number of low angle boundaries that can propagate cracks. Fortunately, these boundaries and cracks run parallel to each other and to the c-axis, so that high field breakdown might be avoided by applying the field parallel to the c-axis or by isolating a single grain.

The second major defect that is easily observed in these samples consists of regions of random precipitates and voids that gives rise to light scattering that is particularly obvious in thick samples which appear black. The wavelength dependence of the relative optical transmission of such thick black samples after removal from the substrate and polishing indicates that the transmission cannot be fitted to a single scattering mechanism. Throughout most of the visible range the transmission is governed by Rayleigh scattering from particles small compared to the wavelengths used. At short wavelengths, approaching the bandgap, transmission may be limited by scattering from particles of size comparable to the wavelength in the crystal or band-tail electronic absorption may be occuring, or both. At longer wavelengths, free carrier absorption again decreases the transmission.

50μ thick crystals grown at 10μ/hr appear blacker than crystals grown at 1μ/hr. A crystal was grown rapidly (30μ/hr) to a thickness of 2mm. The sapphire was ground away and the crystal polished to 50μ thick by grinding on the substrate side only. Transmission optical microscopy revealed non-uniform red-orange to brown regions that ran parallel to the ridges and valleys on the surface.

These are roughly perpendicular to the c-axis and are not associated with the cracks running parallel to the c-axis. Figures 5 (transmitted light) and 6 (surface epi illumination) show that these regions are associated with the surface topology. The coloration is due to light scattering which selectively removes the shorter wavelengths. These scattering regions cannot be detected in crystals grown at 1μ/hr. We attempted to detect these scattering centers directly using scanning electron microscopy, but could not find them, presumably because these were small particles (< 0.5μ) below the resolution limit of the instrument. (The only features observed were several linear series of voids aligned parallel to the c-axis; these may be the traces of the low angle grain boundaries in the growth plane, where the polishing and etching has removed the Ga precipitates and left voids in their place - Figure 7).

In order to detect these scattering particles several 1mm thick samples were removed from their substrates, polished to a thickness of 50μ, then thinned by ion milling to prepare foils for examination by transmission electron microscopy. These observations revealed no second phase particles in slowly-grown crystals (1μ/hr), but in rapidly grown crystals (> 30μ/hr), and then only in regions which appeared colored by transmitted light, small particles (≤ 50 Å) were detected. These always occured only in the regions parallel to the surface ridges, which appeared orange-red by transmitted light. In addition, many voids were detected in these regions. At times, traces of a decorated low angle grain boundary was noted, presumably the same boundaries discussed above. Also very common were stacking faults. (These could not be found in whisker samples.) Outside the regions of precipitation, the crystal perfection was very good and excellent sharp single crystal electron diffraction patterns were obtained.

|← 2500ν →|        FIG. 5



|← 300ν →|        FIG. 6



|← 10ν →|        FIG. 7

To determine whether the low angle grain boundaries and their associated cracks and the local, random, fine precipitation at right angles to the boundaries were in any way associated with chemical impurities, the optical, scanning electron and transmission electron microscopy observations were repeated on crystals grown without the alumina liner, to increase the Si concentration, replacing the liner with a graphite foil liner, and using a zirconia oxygen pump to remove the last traces of oxygen from the growth system. However, no verifiable changes were found in the defect structure already discussed.

These observations were repeated on samples which had been annealed at 1100° in flowing $NH_3$ (see above). Again, no discernible changes in the defect structure could be found.

Finally, crystals were grown on other sapphire orientations and compared with R-plane crystals and with as-grown whiskers. Other sapphire orientations used were single crystal sapphire tubing, and grown sapphire ribbons of orientation $(\bar{1}012)$, $(\bar{1}0\bar{1}0)$ and an unknown plane parallel to $<10\bar{1}2>$. On sapphire, only the $(10\bar{1}0)$ orientation yielded fault-free crystals, see Figure 9 (surface topology by reflected light) vs. normal R-plane growth in Figure 8. These crystals were almost identical to the whiskers. Both this $(10\bar{1}0)$ growth and the whisker growth have one thing in common: they grow with a planar topology, but very slowly.

These results can now be summarized. Slow growth on standard R-plane sapphire can eliminate the small random precipitates in regions following the ridged surface morphology and leading to black crystals. It also reduces the number of low angle grain boundaries and associated cracks as well as the stacking faults, but it does not eliminate them. Planar growth that eliminates the ridged surface morphology - whiskers or on

|←300N→|     FIG. 8 [0001]



|←300N→|     FIG. 9



|←10N→|     FIG. 10
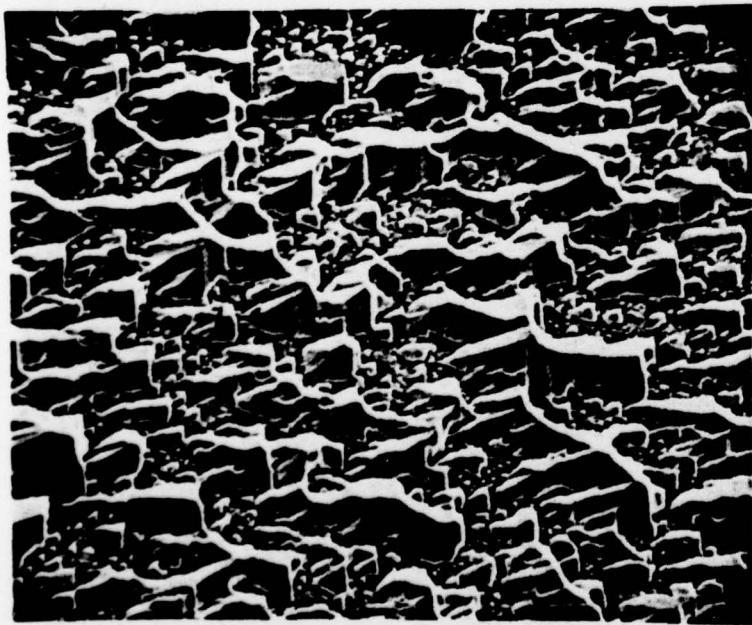


|←300N→|     FIG. 11

(10$\bar{1}$0) sapphire, seems to eliminate all the growth defects, but the growth rates are extremely slow. Growth on R-plane sapphire commences with isolated multi-nucleated islands. Figure 10 is a scanning electron microscope view after only a brief growth period. The crystals are all very well oriented, but as they continue growing and merge together a slight misorientation may lead to the low angle grain boundaries. Secondly the islands are not planar, they already exhibit ridges. As these merge they form the ridged growth surface typical of R-plane growth - see Figure 11 (optical reflection). The dominant plane visible is a slow growth plane. The crystal grows along one of the less prominent planes - a fast growth plane. Hence actual crystal growth is much more rapid in these directions than the average growth rate indicates, and the preponderance of small precipitates and stacking faults orientated parallel to the ridges and valleys probably results from this locally rapid growth.

The implications of these deductions are obvious. We will use the easily-grown R-plane crystals to study and improve chemical and electrically-active center purity, but the samples selected for the high field measurements should be produced by very slow planar growth either on (10$\bar{1}$0) sapphire or as whiskers.

CHARACTERIZATION BY LOW TEMPERATURE LUMINESCENCE

Since the electrical properties of as-grown GaN are dominated by a shallow intrinsic donor, forming an impurity band and causing the crystals to be degenerate at a carrier density of $2\text{-}5 \times 10^{18} \text{cm}^{-3}$, we attempted some low temperature absorption and luminescence measurements at 4.2°K in order to delineate the impurity band and perhaps shed some light on the nature of this band. Instead, we observed a multitude of sharp

lines (some less than 5 meV wide), as though the strong carrier degeneracy were absent. Most of these lines vary from sample to sample and must be due to the various donor and acceptor defects grown into these samples. As described below, we have identified the mechanisms and centers producing these lines: 2 shallow donors, 2 shallow acceptors, and 1 deeper level, probably an acceptor. Yet the chemical identities of these centers are not yet known. Accordingly, we have embarked on a program of ion implanting various commonly expected impurities in order to identify these centers. Whether one of these observed donors is the ubiquitous donor that dominates our as-grown crystals is as yet unknown.

The luminescence was observed on as-grown or annealed samples, left unpolished and unetched on the substrates and immersed in liquid He. Photoluminescence was excited by 3371 $\overset{o}{A}$ radiation from a pulsed $N_2$ laser (100 kw peak power, 10 ns pulse width, 100 pps repetition), filtered by a narrow band pass filter (3371 $\overset{o}{A}$, 50 $\overset{o}{A}$ width) and focussed by a cylindrical lens and a simple lens to a spot size about 2 mm on the sample. (The calculated peak excitation rate in the crystal is about $4 \times 10^{27}$ electron-hole pairs generated per sec per $cm^3$.) The front surface luminescence was filtered by a sharp cut-off low pass solution filter (DDDP iodide in water, 20mg: 100ml, 1 cm path length), focussed onto the entrance slit of a Perkin-Elmer El f/8 monochromator and detected by either an EMI 6256S or a cooled EMI 9558B photomultiplier.

The resulting signals were processed either with a lock-in amplifier tuned to a 500 hz chopper in the luminescence beam or with a boxcar integrator triggered by the laser pulses.

Figures 12-17 are the raw spectra near the bandgap for several as-grown or annealed samples. Figure 18 schematically summarizes the observed bands and the interpretation is given in Table 1.

DW 201 GaN sample at LHe
slit = 900 μm
Gain. = 200 μV

⊢⊣ 1.26 mev

LHe, N₂ Laser

$\Delta E = 5$ mev →

3675Å (3.4671 ev)
3572 Å (3.4700 ev)
3566 Å (3.4758 ev)

3625Å (3.4193 ev)
3619Å (3.4249 ev)
3613Å (3.4306 ev)
3603 A (3.4400 ev)
3598 Å (3.4449 ev)
3585 Å (3.4570 ev)

3682 Å (3.3660 ev)
3669 Å (3.3780 ev)
3663 Å (3.3840 ev)
3645Å (3.4000 ev)

3794Å (3.2644 ev)
3773Å (3.2840 ev)
3756Å (3.2990 ev)

BEST AVAILABLE COPY

λ(Å) ←

19

FIG. 12
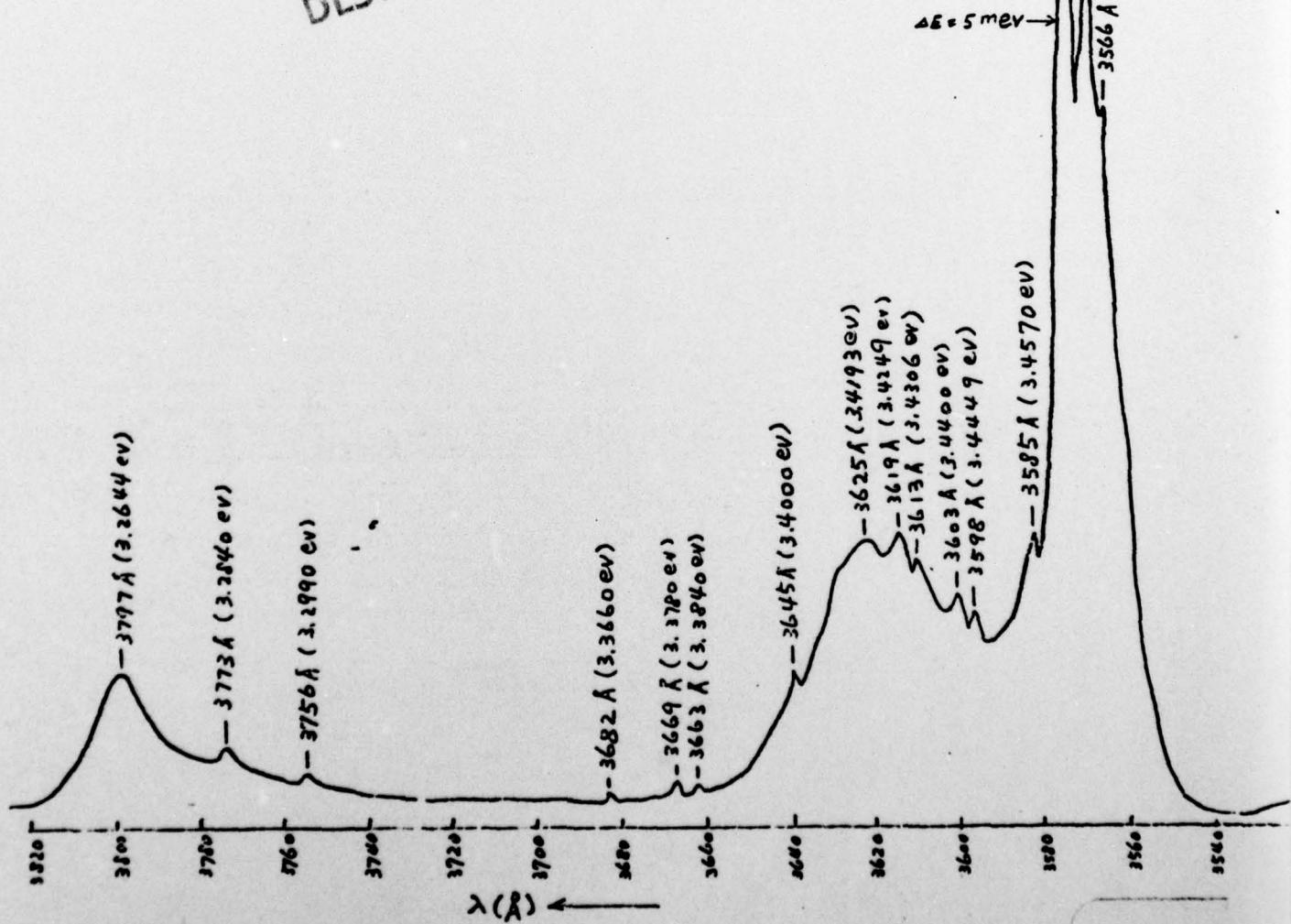
DW201 GaN Single Crystal
at LHe. N₂ Laser
slit = 900 μm
Gain = 200 μV

→|←— 1.26 meV

BEST AVAILABLE COPY

3905 Å (3.1741 eV)
3797 Å (3.2644 eV)
3773 Å (3.2840 eV)
3756 Å (3.2990 eV)
3652 Å (3.3960 eV)
3649 Å (3.3980 eV)
3643 Å (3.3040 eV)
3625 Å (3.4193 eV)
3619 Å (3.4249 eV)
3613 Å (3.4306 eV)
3603 Å (3.4400 eV)
3598 Å (3.4449 eV)
3591 Å (3.4516 eV)
3575 Å (3.4670 eV)
3575 Å (3.4671 eV)
3572 Å (3.4700 eV)
3566 Å (3.4758 eV)

λ (Å)
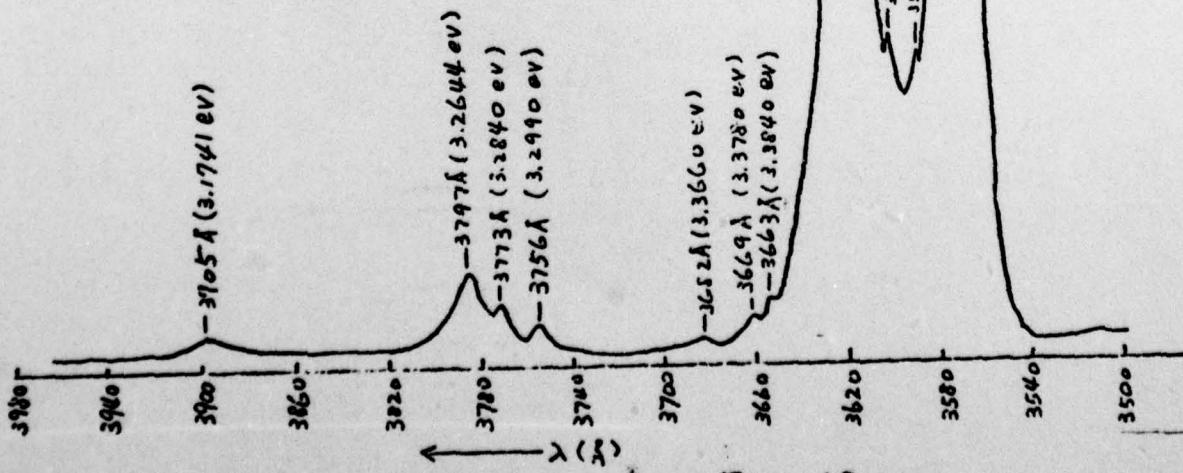
FIG. 13

DW408 GaN single crystal
slit = 900 μm
Gain = 500 μV

LHe , N₂ Laser

—⊣⊢— 1.26 meV

3905 Å (3.1741 eV)
3797 Å (3.2644 eV)
3773 Å (3.2840 eV)
3756 Å (3.2990 eV)
3682 Å (3.3660 eV)
3669 Å (3.3780 eV)
3625 Å (3.4193 eV)
3619 Å (3.4249 eV)
3613 Å (3.4306 eV)
3603 Å (3.4400 eV)
3598 Å (3.4449 eV)
3591 Å (3.4516 eV)
3566 Å (3.4758 eV)
3575 Å (3.4671 eV)
3572 Å (3.4700 eV)

λ (Å)
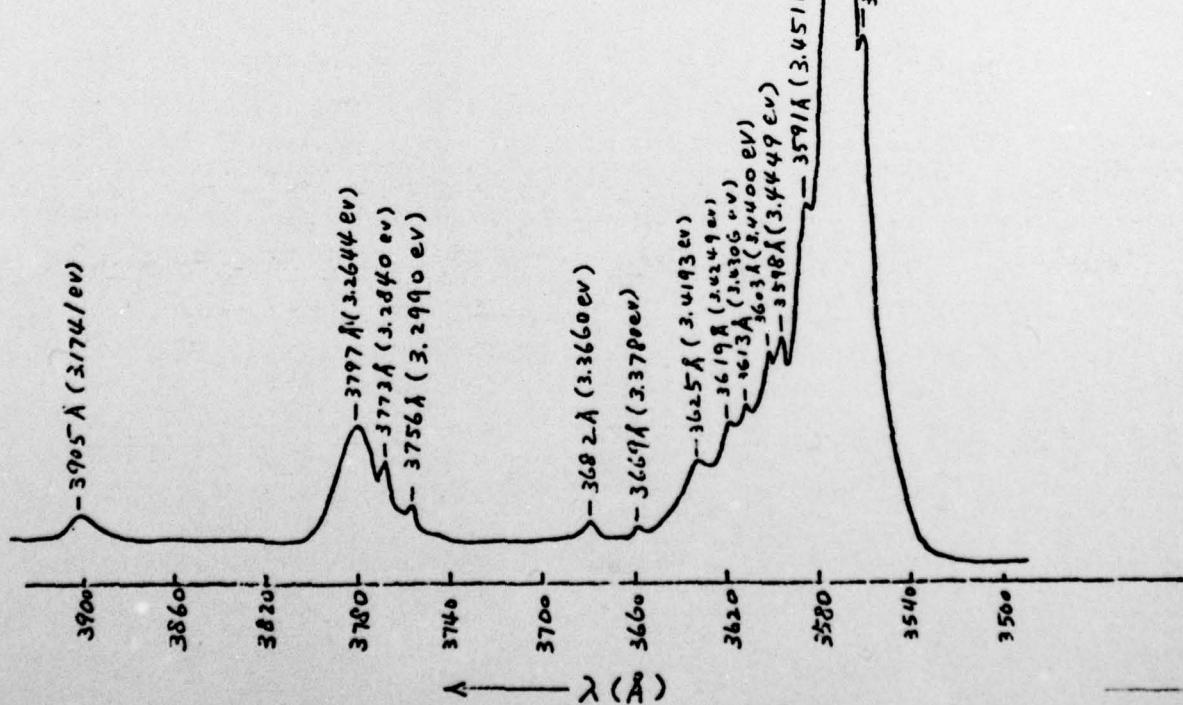
FIG. 14

DW602 GaN single crystal
(with Annealing)

Slit = 600μm
Gain = 500μV

⊢─────┤ 0.84 mev

LHe, N₂ Laser

3800Å (3.2619 eV)
3773Å (3.2840 eV)
3756Å (3.2990 eV)
3700Å (3.3500 eV)
3678Å (3.3701 eV)
3650Å (3.3959 eV)
3626Å (3.4184 eV)
3613Å (3.4306 eV)
3601Å (3.4421 eV)
3575Å (3.4671 eV)
3538Å (3.5038 eV)

λ (Å)

BEST AVAILABLE COPY

FIG. 15

-22-
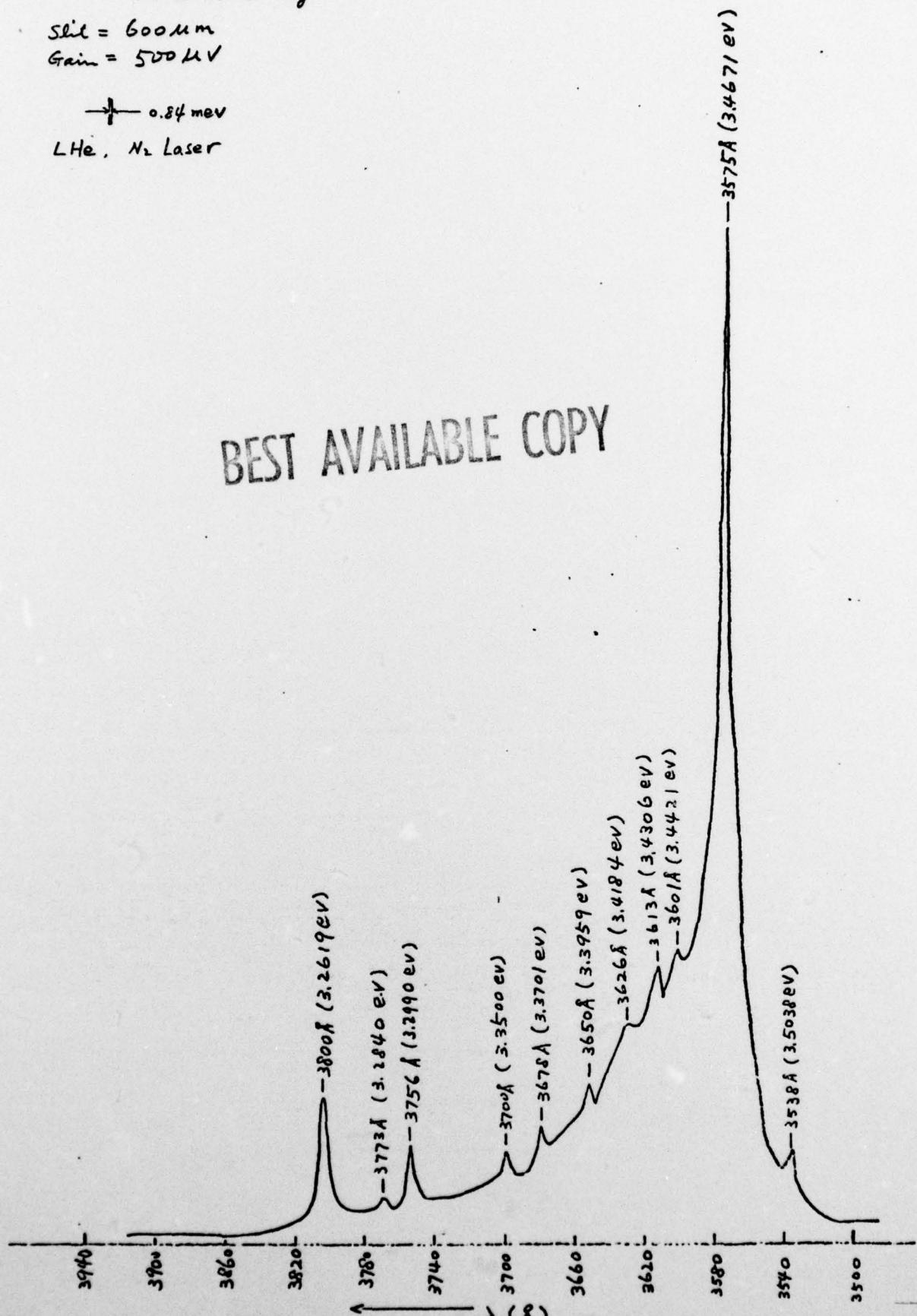
DW203 GaN single crystal
Θ∠He . N₂ Laser
slit = 650 μm
Gain = 200 μV

$\longmapsto$ 0.91 meV

BEST AVAILABLE COPY

3654Å (3.3921 ev)

3622Å (3.4221 ev)
3619Å (3.4249 ev)
3614Å (3.4297 ev)
3603Å (3.4400 ev)
3598Å (3.4449 ev)
3586Å (3.4564 ev)
3576Å (3.46615 ev)
3572Å (3.4700 ev)
3565Å (3.4768 ev)

3622Å (3.4221 ev)
3619Å (3.4249 ev)
3614Å (3.4297 ev)
3603Å (3.4400 ev)
3598Å (3.4449 ev)
3586Å (3.4564 ev)
3576Å (3.4662 ev)
3571Å (3.4710 ev)

3678Å (3.3704 ev)

3672Å (3.3755 ev)

3654Å (3.3921 ev)

3700  3680  3660  3640  3620  3600  3580  3560  3540

3860  3820  3780  3740  3700  3660  3620  3580  3540  3500

$\longleftarrow$ λ (Å)

FIG. 16

-23-

DW214 GaN Single Crystal
∠ He, N₂ Laser
slit = 700 μm
⊢—⊣ 0.98 meV

BEST AVAILABLE COPY

−3617Å (3.4268 eV)

−3591Å (3.4516 eV)
−3575Å (3.4671 eV)
−3572Å (3.4700 eV)

−3905Å (3.174 eV)

−3797Å (3.2644 eV)

with Annealing
(G = 2 mV)

without Annealing
(G = 500 μV)

3940  3900  3860  3820  3780  3740  3700  3660  3620  3580  3540  3500

← λ (Å)

FIG. 17

−24−

(a) liner: Alumina tube  (d) thickness: 100-150 μm
(b) NH₃ gas: Air products  (e) color: Transparent
(c) Substrate: Sapphire tube

(a) Alumina  (d) 150-200 μ
(b) Air products  (e) black
(c) Sapphire tube

(a) Alumina  (d) 200 μ
(b) Air products  (e) black
(c) Sapphire  (f) polycrystalline

(a) Alumina tube  (d) 150 μm
(b) Air products  (e) grey
(c) sapphire R plane

(a) Alumina tube  (d) 100 μ
(b) Air products  (e) grey
(c) sapphire plane

(a) Alumina tube
(b) Matheson NH₃
(c) sapphire plane
(d) 150 μm
(e) black

(a) quartz tube
(b) Air products
(c) sapphire plane
(d) 150 μ
(e) Transparent

3.20   3.25   3.30   3.35   3.40   3.45   3.50

⟶ hν (ev)

FIG. 18

BEST AVAILABLE COPY

-25-

## TABLE 1

### NEAR EDGE LUMINESCENCE IN GaN AT 4.2°K

| | |
|---|---|
| 3.4758 eV | Free exciton |
| 3.4700 | Exciton bound to neutral donor 1 (n=1) |
| 3.4671 | Exciton bound to neutral donor 2 (n=1) |
| 3.4570 | Exciton bound to neutral acceptor 1 |
| 3.4516 | Exciton bound to neutral acceptor 2 |
| 3.4449 | n=2 decay of exciton bound to donor 1 |
| 3.4400 | n=3 decay of exciton bound to donor 1 |
| 3.4306 | n=2 decay of exciton bound to donor 2 |
| 3.4249 | n=3 decay of exciton bound to donor 2 |
| 3.4193 | Exciton bound to deep level |
| 3.4000 | Exciton bound to donors 1 & 2 - TO phonon |
| 3.3840 | Free exciton - LO phonon |
| 3.3780 | Exciton bound to donors 1 & 2 - LO phonon |
| 3.3660 | Exciton bound to acceptors 1 & 2 - LO phonon |
| 3.2990 | Free exciton - 2 LO phonons |
| 3.2840 | Exciton bound to donors 1 & 2 - 2 LO phonons |
| 3.2644 | Donor-acceptor pair emission |
| 3.1741 | Donor-acceptor pair - LO phonon |

Although GaN crystallizes in the wurtzite structure, the anisotropies
in most properties, e.g. effective masses, dielectric tensor, appear to
be very small. Hence, in the first order interpretation that follows,
we assume that GaN is isotropic.

Simple effective mass theory predicts that the binding energy of
a free exciton (not bound to any lattice center) should be about 30 meV
relative to an unbound electron-hole pair at the zone center. From the
known bandgap of GaN at 4.2°K (from absorption and reflectivity) we know
then where to look for the free exciton decay emission and an emission
peak does occur very close to this energy at 3.4758 eV (see Table I),
enabling us to identify it as the free exciton peak and yielding a free
exciton binding energy of 28 meV. As expected, this peak is replicated
by the simultaneous emission of one and two LO phonons (measured LO phonon,
90 meV; previously determined from reststrahlen measurements, 91 meV).

With the extremely high excitation powers used, we expect all
ionized donors and acceptors to be neutralized by free carriers. Again
using effective mass theory, we predict a hydrogen-like donor state
ionization of 30 meV and an acceptor roughly 5-10 times deeper than this,
the latter due to a large, but currently uncertain hole mass. Excitons
should bind to both neutral donors and neutral acceptors and the binding
energies (relative to the free exciton) should be linearly related to the
ionization energies of the donors and acceptors, the Haynes rule, with
the proportionality constant usually 0.1 to 0.2 in other materials.

Two lines are observed close to the region for the decay of excitons
bound to neutral donors. These lines vary independently in intensity
from sample to sample. Hence the centers are not intrinsic. Associated
with each of these lines are at least 2 other lines of lower intensities
at lower energies. The latter are interpreted as 2 electron transitions,

-27-

in which the donor is left in the n=2 and n=3 excited hydrogenic state after the radiative transition, rather than in the n=1 ground state.  Deviations from effective mass theory (central cell corrections) normally perturb the compact ground state much more than they do the extended excited states.  Hence we can assume that the n=3 state energy is given accurately by the effective mass approximation.  Then the separation between the n=3 line and the n=1 ground state line can be added to this to yield the normal donor ionization energy.  This yields 36 and 41 meV respectively for the two observed donors.  (The deduced Haynes Rule constant here lies between 0.15 and 0.20.)  These lines are also replicated by TO (70 meV) and LO (90 meV) phonons.

In the bound exciton to neutral acceptor region at least two extrinsic lines are also observed, but these are not associated with any observed two electron transitions.  Using Haynes Rule, we estimate that the ionization energies of these two acceptors lie between 200 and 300 meV, very deep indeed for a "shallow level".  These lines are replicated by LO phonons.  A third extrinsic line is sometimes observed just beyond this region.  This is probably an exciton bound to a deeper level, again probably an acceptor with a deduced ionization energy of ~ 0.5 eV.

At lower energies, phonon replicated donor-acceptor peaks appear, the direct recombination of electrons bound to the two neutral donors with holes bound to the acceptors.

Apart from the free exciton line, all the peaks discussed are extrinsic, that is, they vary in intensity from sample to sample.  Several correlations have been made, but none that has led to any firm conclusions yet.  The deep acceptor peak is enhanced in samples that appear very black due to the presence of precipitates and also in samples grown when graphite

was present in the growth chamber. The use of a poor grade of $NH_3$ during growth enhances some of the donors and acceptors. Li diffused samples are dominated by a broad emission at 2.13 eV, probably some complex defect involving Li, but no simple donor or acceptor can be seen. Annealing in flowing $NH_3$ (1100°, 5 hours) has no effect on the electrical carrier concentration nor on the luminescence line widths, but it does improve the luminescent efficiencies of all peaks uniformly by a factor of 5 to 10. This then must reduce the number of bulk or surface non-radiative recombination states. In comparing older samples, heavily Si doped, $n = 5 \times 10^{19} cm^{-3}$ with the less heavily doped more recent samples $n = 2-5 \times 10^{18} cm^{-3}$, it is evident that the bound exciton line widths have been decreased from 6-10 meV to less than 5 meV. If these widths are lifetime determined, the purer crystals correspond to a lifetime of $1 \times 10^{-12}$ sec. This is too short to be a bound exciton Auger recombination lifetime. It is probably being determined by interaction with the free electrons in this degenerate material. Hence even if none of these observed lines turn out to be due to the dominant intrinsic donor, we may have an indirect way of studying that level.

We are currently engaged in a doping program, intentionally adding expected common impurities, Si, C, O, S, Zn, Na, etc., both by ion implantation and during growth in our first CVD apparatus, in an attempt to identify these as-grown defects chemically.

One final observation: if there are no shallower acceptors in GaN than those already identified here, than it is obvious why low resistivity p-type material has never been observed. The acceptors are simply too deep to exhibit much hole ionization at room temperature. If we can identify these levels and learn to dope with them, then high temperature Hall effect measurements should confirm this conclusion.

## DISTRIBUTION LIST

### Contract N00014-75-C-0295

| | |
|---|---|
| Chief of Naval Research<br>Attn: Code 427<br>Arlington, VA 22217 | 3 copies |
| Chief of Naval Research<br>Attn: Code 105<br>Arlington, VA 22217 | 6 copies |

Director
Naval Research Laboratory
Washington, DC 20375

| Attn: Code 2627 | 6 copies |
|---|---|
| 5220 | 1 copy |
| 5220 | 1 copy |
| 6400 | 1 copy |

| | |
|---|---|
| Defense Documentation Center<br>Building 5<br>Cameron Station<br>Alexandria, VA 22314 | 12 copies* |
| Advisory Group on Electron Devices<br>9th Floor<br>201 Varick Street<br>New York, NY 10014 | 1 copy |
| Texas Instruments, Inc.<br>P.O. Box 5012<br>Dallas, TX 75222<br>Attn: Dr. Robert W. Haisty | 1 copy |
| University of Southern California<br>School of Engineering<br>Department of Materials Science<br>University Park<br>Los Angeles, CA 90007<br>Attn: Prof. M. Gershenzon | 1 copy |
| Office of the Director of Defense<br>Research and Engineering<br>Information Office Library Branch<br>The Pentagon<br>Washington, DC 20301 | 1 copy |

U.S. Army Research Office                    1 copy
Box CM, Duke Station
Durham, NC    27706

Director, National Bureau of Standards  1 copy
Attn:  Technical Library
Washingotn, DC    20234

Commanding Officer                           1 copy
Office of Naval Research Branch Office
536 Clark Street
Chicago, IL    60605

Air Force Cambridge Research Laboratory 1 copy
L.G. Hanscom Field
Technical Library
Cambridge, MA    02138

Harry Diamond Laboratories                   1 copy
2800 Powder Mill Road
Adelphia, MD    20783
Attn:  Technical Library

Commandant, Marine Corps                     1 copy
Scientific Advisor (Code AX)
Washington, DC    20380

Naval Postgraduate School                    1 copy
Technical Library (Code 0212)
Monterey, CA    93940

Naval Missile Center                         1 copy
Technical LIbrary (Code 5632.2)
Point Mugu, CA    93010

Naval Ocean Systems Center                   1 copy
Code 922/H. Wieder
San Diego, CA    92152

Naval Weapons Laboratory                     1 copy
Technical Library
Dahlgren, VA    22448

North Carolina State University              1 copy
Electrical Engineering Department
Attn:  Prof. M. A. Littlejohn
Raleigh, NC    27607

RCA Laboratories
David Sarnoff Research Center
Princeton, NJ    08540
Attn:  Dr. Y. Narayan                          1 copy
       Dr. J. Pankove                          1 copy

Raytheon Company                               1 copy
Research Division
28 Seyon Street
Waltham, MA    02154

Naval Avionics Facility                        1 copy
Technical Library
Indianapolis, IN    46218

Air Force Office of Scientific Research    1 copy
Department of the Air Force
Washington, DC    20333

Commanding Officer                             1 copy
Office of Naval Research Branch Office
1030 East Green Street
Pasadena, CA    91101

Director                                       1 copy
U.S. Army Engineering Research and
    Development Laboratories
Fort Belvoir, VA    22060
Attn:  Technical Documents Center

Air Force Avionics Laboratory                  1 copy
Air Force Systems Command
Technical Library
Wright-Patterson Air Force Base
Dayton, OH    45433

Director                                       1 copy
Defense Advanced Research Projects
    Agency
Attn:  Technical Library
1400 Wilson Boulevard
Arlington, VA    22209